

RELATIVISTIC EFFECTS IN EXTREME MASS RATIO GRAVITATIONAL WAVE BURSTS

NICOLÁS YUNES

Institute for Gravitational Physics and Geometry, Center for Gravitational Wave Physics, Department of Physics, Pennsylvania State University, University Park, PA 16802

CARLOS F. SOPUERTA

Department of Physics, University of Guelph, Guelph, Ontario, Canada N1G 2W1

LOUIS J. RUBBO AND KELLY HOLLEY-BOCKELMANN

Center for Gravitational Wave Physics, Pennsylvania State University, University Park, PA 16802

Draft version June 21, 2024

ABSTRACT

Extreme mass ratio bursts (EMRBs) have been proposed as a possible source for future spaceborne gravitational wave detectors, such as the Laser Interferometer Space Antenna (LISA). These events are characterized by long-period, nearly-radial orbits of compact objects around a central massive black hole. The gravitational radiation emitted during such events consists of a short burst, corresponding to periaapse passage, followed by a longer, silent interval. In this paper we investigate the impact of including relativistic corrections to the description of the compact object's trajectory via a geodesic treatment, as well as including higher-order multipole corrections in the waveform calculation. The degree to which the relativistic corrections are important depends on the EMRB's orbital parameters. We find that relativistic EMRBs ($v_{\max}/c > 0.25$), are not rare and actually account for approximately half of the events in our astrophysical model. The relativistic corrections tend to significantly change the waveform amplitude and phase after only one orbit relative to a Newtonian description. The dephasing is of particular importance not only to gravitational wave detection, but also to parameter estimation, since it is highly correlated to the spin of the massive black hole. Consequently, we postulate that if a relativistic EMRB is detected, such dephasing might be used to probe the relativistic character of the massive black hole and obtain information about its spin.

Subject headings: black hole physics — Galaxy: nucleus — gravitational waves — stellar dynamics

1. INTRODUCTION

Low-frequency ($10^{-5} \lesssim f \lesssim 0.1$ Hz) gravitational wave interferometers, such as the proposed Laser Interferometer Space Antenna (LISA) (Bender et al. 1998; Danzmann & Rüdiger 2003; Sumner & Shaul 2004), will open a completely new window to the Universe. Through observations of low-frequency gravitational radiation we will be able to witness the inspiral and merger of massive black hole binaries; the inspiral of compact objects into massive black holes; and millions of quasi-stationary compact galactic binaries. Recently, a new source of low-frequency gravitational radiation has been suggested: extreme mass ratio bursts (EMRBs) (Rubbo et al. 2006, 2007).

EMRBs consist of a stellar-mass compact object (SCO) orbiting a massive black hole (MBH) of $10^{4-8} M_{\odot}$ with orbital periods greater than $T_{\text{cut}} = 3 \times 10^4$ s. The defining orbital period cutoff is derived from LISA's lower frequency limit of $f_{\text{cut}} = 3 \times 10^{-5}$ Hz. Systems with orbital periods less than T_{cut} will radiate continuously inside the LISA band. Such continuous systems are more appropriately categorized as extreme mass ratio inspirals (EMRIs) and have been studied extensively elsewhere: recent estimations of the event rate are given by Gair et al. (2004) and Hopman & Alexander (2006); a discussion on a possible EMRI background is given by Barack & Cutler (2004a); accounts on the theoretic

cal description of EMRIs can be found in the reviews by Poisson (2004) and Glampedakis (2005), while the recent review by Amaro-Seoane et al. (2007) describes the astrophysical and detection applications.

Although EMRB events are distinct from EMRI events, their evolutionary track could be connected. In the burst scenario, the SCO orbits the MBH emitting a beamed burst of gravitational radiation during pericenter passage. The emitted radiation carries away energy and angular momentum from the system so that after multiple pericenter passages the orbital period decreases, and possibly the system becomes an EMRI. However, this evolutionary track is most likely disrupted by scattering interactions with other stars and/or if the SCO plunges directly into the central MBH on one of its passages.

The EMRB event rate has recently been investigated using simplified galactic models and data analysis techniques (Rubbo et al. 2006, 2007; Hopman et al. 2006). Using a density profile described by an η -model (Tremaine et al. 1994), Rubbo et al. (2006, 2007) suggested an event rate of $\sim 15 \text{ yr}^{-1}$ for events with signal-to-noise ratios (SNRs) greater than five out to the Virgo cluster. When mass segregation and different inner cusp models are considered, the predicted rate decreases by an order of magnitude (Hopman et al. 2006). These preliminary studies were aimed at understanding if EMRB event rates are interesting for low-

frequency gravitational wave detectors such as LISA. More work is still needed to improve the predicted event rate in the context of realistic galaxies, where the role of non-equilibrium dynamics, anisotropy, complex star formation histories, substructure, and non-sphericity may act to change the rate from these fiducial estimates by orders of magnitude (Holley-Bockelmann & Sigurdsson 2006; Rubbo et al. 2006, 2007).

In addition to the astrophysical uncertainties, there are no investigations of the impact of relativistic corrections to EMRB dynamics. All EMRB studies have been carried out in a *quasi-Newtonian* framework. In this framework, one uses the Newtonian equations of motion and extracts the gravitational waveforms by means of the *quadrupolar* approximation formula. This approximation ignores the black hole nature of the central potential including the black hole’s rotation (spin). Moreover, the quasi-Newtonian approach is technically valid only for orbits with non-relativistic velocities. However, a considerable number of EMRBs are characterized by large pericenter velocities ($v_p \gtrsim 0.25c$). These *relativistic* EMRBs will produce gravitational wave signals with larger SNRs as will be shown later. Consequently, the estimated event rates using only a Newtonian treatment become lower limits.

In this paper, we study the effects of relativistic corrections to EMRB events. For extreme-mass-ratio systems a simple way of introducing relativistic corrections is by using the so-called *semi-relativistic* approximation introduced by Ruffini & Sasaki (1981), and used recently in the context of EMRIs by Gair et al. (2005, 2006). In this approximation, the MBH and surrounding area are modeled using the Kerr solution to Einstein’s field equations, which describes a stationary spinning black hole (the Schwarzschild solution corresponds to the non-spinning case). The SCO is considered to be a point-like object (neglecting its own self-gravity) whose trajectory is described by a geodesic of the Kerr spacetime. In other words, we have replaced the Newtonian equations of motion by relativistic geodesic equations of motion.

The relativistic description introduces effects such as orbital precession and frame dragging, but it does not account for effects due to the gravitational field induced by the SCO. These effects, for example, lead to changes in the (geodesic) constants of motion due to radiation reaction. Even though these effects introduce errors that scale with the system’s mass ratio (e.g. see Glampedakis 2005), they cannot be neglected for EMRIs. This is because in the late stages of the EMRI the SCO spends a substantial fraction of cycles in the strong-field region of the MBH. On the other hand, in the case of EMRBs, the SCO sling-shots around the MBH and its interaction time during pericenter passage is relatively small ($\sim 10^5$ s). Radiation reaction effects can then be neglected in EMRBs since the radiation reaction timescale is always much larger than the period of pericenter passage.

In this paper we also improve on the semi-relativistic approximation by using a more precise gravitational wave extraction procedure. The procedure employed is the multipole-moment wave generation formalism for slow-motion objects with arbitrarily strong internal gravity (Thorne 1980). We consider terms up to the mass-octopole and current-quadrupole multipoles, thus im-

proving on the mass-quadrupole analysis of Rubbo et al. (2006, 2007) and Hopman et al. (2006). Higher multipoles will become important if the system becomes even more relativistic, but pericenter velocities for EMRBs are typically small to moderate relative to the speed of light (typically $0.1 \lesssim v_p/c \lesssim 0.5$). In the case of EMRIs, where one strives to track the phase evolution accurately, the gravitational waves produced in the strong field region of the MBH require techniques from black hole perturbation theory (Poisson 2004; Glampedakis 2005) that we shall not consider here.

The study of the relativistic corrections considered in this work leads to the following conclusions. First, we find that relativistic effects are significant for approximately 50% of the orbits contained in the EMRB phase space considered by Rubbo et al. (2006, 2007). These relativistic EMRB orbits differ from their Newtonian counterparts in such a way that the associated waveforms present a noticeable different structure. In particular, we find that there is a dephasing relative to Newtonian waveforms that is due to precessional effects that depend strongly on the MBH spin. These findings show that EMRB events are relativistic enough that they should be treated accordingly, as was previously found for EMRIs (Glampedakis 2005).

Second, we find that the corrections to the trajectories affect the waveforms much more than the corrections in the waveform generation. For example, for a given relativistic trajectory, we find that the difference between the SNR of a waveform obtain from the quadrupole formula to that obtained from the quadrupole-octopole formula is of the order of 1%. On the other hand, using the same waveform generation formula (quadrupole or quadrupole-octopole), the difference between the SNR of a Newtonian waveform to that of a Kerr waveform is $\sim 200\%$. These findings show that modeling EMRB waveforms with a quasi-Newtonian treatment might not be sufficient.

Third, we find that the relativistic corrections accumulate with multiple bursts and, thus, they may be important for parameter estimation studies. Interestingly, for relativistic EMRBs such corrections may be used to determine or bound the spin of the MBH if a high SNR event is detected. Furthermore, if parameters can be determined accurately enough, it might also be possible to use EMRB measurements to test deviations from General Relativity. The connection between the SNR and the accuracy in the determination of the MBH spin requires a more detailed data analysis study that shall be carried out elsewhere.

The remainder of this paper is divided as follows: Section 2 deals with the dynamics of EMRBs in the semi-relativistic approximation and justifies the use of this approximation for these systems; Section 3 reviews the inclusion of higher-order multipolar corrections to the waveform generation formalism; Section 4 describes the numerical implementation of the equations of motion and the initial data used; Section 5 compares the orbital trajectories and waveforms in the time domain; Section 6 concludes and points to future research.

In this paper, we denote the MBH mass by M_\bullet and its *gravitational radius* by $R_\bullet = 2GM_\bullet/c^2$, where c is the speed of light and G the Newtonian gravitational constant. To simplify some expressions we normalize masses

with respect to $M_{\text{MW}} = 4 \times 10^6 M_{\odot}$, which is of the same magnitude as the mass of the MBH at the center of the Milky Way (Ghez et al. 2005). The gravitational radius can then be written as:

$$R_{\bullet} = (3.82 \times 10^{-7} \text{ pc}) \frac{M_{\bullet}}{M_{\text{MW}}}. \quad (1)$$

2. EMRB DYNAMICS

In this section, we describe the formalism employed to describe the orbital motion. Newtonian dynamics usually provides an adequate description of many astrophysical sources of gravitational waves, at least from a qualitative point of view. However, for certain gravitational wave sources, such a description is insufficient and relativistic effects have to be considered. For EMRB sources with pericenter distances and velocities near $r_p > 4R_{\bullet}$ and $v_p/c < 0.5$, the semi-relativistic approximation to the equations of motion, in combination with a multipolar description of the gravitational radiation, can adequately model the dynamics and gravitational radiation, as we argue below.

The semi-relativistic approximation treats the motion of the SCO in the point-particle limit as a geodesic of the MBH geometry, which is justified based on the small mass-ratios associated with these systems. In this work, we adopt Cartesian Kerr-Schild coordinates, $\{t, x^i\}$ ($i = 1, 2, 3$), in which the MBH geometry is time-independent, reflecting its stationary character, and tends to a flat-space geometry in Cartesian coordinates far from the MBH. We denote the geodesic trajectory by $z^i(t)$, its spatial velocity by $v^i(t) = dz^i/dt$, and its spatial acceleration by $a^i(t) = dv^i/dt$. The later, in such a coordinate system, and by virtue of the geodesic equations of motion, has the following form (e.g. see Marck 1996):

$$a^i = F^i[v^j; g_{\mu\nu}, \partial_j g_{\mu\nu}], \quad (2)$$

where $g_{\mu\nu}$ ($\mu, \nu = 0, 1, 2, 3$) are the spacetime components of the MBH metric. These equations describe the influence of the spacetime curvature produced by the MBH and approach the Newtonian equations of motion in the regime where $v/c = |v^i|/c \ll 1$ and $GM_{\bullet}/(c^2 r) \ll 1$ ($r = |x^i|$).

The effects from the self-gravity of the SCO can be neglected. To see consider the (Keplerian) orbital timescale, T_{orb} , in comparison to a characteristic radiation-reaction timescale, T_{rr} . For the latter, we can use the timescale associated with the rate of change for the semi-latus rectum, p , as related to the pericenter distance by $r_p = p/(1+e)$, namely $T_{\text{rr}} \sim p/|dp/dt|$. The radiation-reaction timescales of the other orbital elements are comparable or larger (see, e.g. Glampedakis 2005). The ratio of these timescales is

$$\frac{T_{\text{orb}}}{T_{\text{rr}}} \sim 2\pi\mu \left(\frac{R_{\bullet}}{2p} \right)^{5/2}, \quad (3)$$

where $\mu = m/M_{\bullet}$ is the mass ratio of the system and m the SCO mass. It is evident that the radiation-reaction timescale is much greater than the orbital timescale due to the extreme mass ratio, $\mu \ll 1$, and because EMRBs have $p \gg \mu^{5/2} R_{\bullet}$. In the unlikely case that more accuracy is required, one could improve the analysis through the use of ‘‘Kludge’’ waveforms (Babak et al.

2007), which have been shown to reproduce numerical results in the adiabatic approximation accurately for EMRIs.

Formally, the orbital timescale used is not really the exact timescale of orbital motion. This is because the mass distribution of a MBH-embedded galaxy possesses a non-Keplerian potential that leads to non-Keplerian orbits. However, most EMRBs (by rate) have apocenters that do not extend far into the stellar population, implying that the contribution from the galaxy potential is minimal. The orbits we study in later sections have a contamination from the galactic potential that is less than 2% of the MBH mass. Moreover, Hopman et al. (2006) rightly argue that the inner region is statistically empty of stars, which is due to finite effects realized at the small scales observed near the MBH.

Certain constraints may be derived on the size of p and r_p for EMRB events. The most important constraint is derived from the definition of EMRBs: orbits with sufficiently large orbital period $T_{\text{orb}} > T_{\text{cut}}$. Assuming a Keplerian orbit (which is a rough assumption), this constraint translates to pericenter distances as follows

$$r_p > (7.98 \times 10^{-7} \text{ pc}) \frac{(1-e)}{0.1} \left(\frac{M_{\bullet}}{M_{\text{MW}}} \right)^{1/3} \left(\frac{T}{T_{\text{cut}}} \right)^{2/3}, \quad (4)$$

where we have rescaled quantities assuming a typical eccentricity of $e = 0.9$ (Rubbo et al. 2006, 2007) and a typical MBH mass of $M_{\bullet} = M_{\text{MW}}$. In terms of geometrized units, such a constraint translates roughly to $r_p > 2R_{\bullet}$.

This constraint can be compared with the requirement that the SCO does not get captured. The SCO would be captured if it crossed the black hole event horizon, located (in Boyer-Lindquist coordinates) at

$$r_{\text{cap}} = (1.91 \times 10^{-7} \text{ pc}) \frac{M_{\bullet}}{M_{\text{MW}}} \left[1 + \sqrt{1 - \frac{a_{\bullet}^2}{M_{\bullet}^2}} \right], \quad (5)$$

where a_{\bullet} is the (Kerr) MBH spin parameter, related to its intrinsic angular momentum by $S_{\bullet} = GM_{\bullet} a_{\bullet}/c$, and bounded by $a_{\bullet}/M_{\bullet} \leq 1$. Thus, for a maximally spinning Kerr MBH ($a_{\bullet} = M_{\bullet}$), $r_{\text{cap}} = 0.5R_{\bullet}$, while for a Schwarzschild (non-spinning) MBH it is just R_{\bullet} . This condition tell us simply that $r_p > r_{\text{cap}}$, which is a condition superseded by the constraint on the orbital period given in equation (4). One could explore other possible constraints (Rubbo et al. 2006, 2007) but they are in general superseded by equation (4).

These constraints clearly exclude the ergosphere of the MBH ($r_{\text{cap}} < r \lesssim R_{\bullet}$) where frame dragging effects are most pronounced. However, for EMRIs it has been argued (Glampedakis 2005) that orbits with $r_p < 10R_{\bullet}$ cannot be considered Keplerian anymore, mainly due to precessional effects. This statement can be made more quantitative by looking at the ratio of the first-order post-Newtonian (1 PN) expression for the energy of a circular orbit (Blanchet 2006) to its Newtonian value, which scales as $7R_{\bullet}/(8r_p)$ for extreme-mass ratios. For example, for orbits with pericenter passage $r_p \sim 5R_{\bullet}$, the 1 PN correction is already approximately 20% relative to the Newtonian value. This indicates that, even for orbits outside the ergosphere, relativistic effects are not necessarily negligible.

The relativistic geodesic equations of motion introduce

corrections to the Newtonian motion that can be interpreted in terms of a black hole *effective* potential. By comparing the Newtonian and relativistic potentials one can see that the relativistic corrections dominate over the centrifugal barrier at small distances from the black hole center. In this work we show that these relativistic corrections can be sampled by EMRBs and hence, one should model these systems accordingly. Nevertheless, as we argued above, the relativistic treatment of EMRBs does not need to be as sophisticated as in the case of EMRIs, since radiation-reaction can be neglected.

3. EMRB WAVEFORMS

In this section we describe how we extract gravitational waveforms once we have integrated the geodesic equations of motion. We use a multipole-moment wave generation formalism for slowly-moving objects with arbitrarily strong internal gravity (Thorne 1980; Flanagan & Hughes 2005; Glampedakis 2005). In quasi-Newtonian and semi-relativistic treatments, the radiation is modeled by the lowest non-vanishing multipole moment: the mass-quadrupole. To that order, and for the case of a point-like object orbiting a MBH at a fixed coordinate location, the plus and cross polarizations are given by (Misner et al. 1973; Thorne 1980)

$$h_{+, \times} = \frac{2Gm}{rc^4} \epsilon_{+, \times}^{ij} (a_i z_j + v_i v_j), \quad (6)$$

where r is the (flat-space) distance to the observer and $\epsilon_{+, \times}^{ij}$ are polarization tensors. This expression assumes, based on the slow motion approximation, that the change in the acceleration with respect to time, the *jerk*, $j^i = da^i/dt$, is a small quantity. More precisely, we are neglecting terms of order $(v/c)^3$, or in other words, since the (quadrupole) leading order terms are of order $(v/c)^2$, this implies a relative error of order v/c .

One can improve on this description for the gravitational radiation by accounting for higher-order multipole moments. In this paper, we consider the mass-octopole and current-quadrupole multipoles, which require the knowledge of one more time derivative of the trajectory, the *jerk*. Adding these contributions to equation (6), the gravitational waveforms are given by

$$\begin{aligned} h_{+, \times} = & \frac{2Gm}{rc^4} \epsilon_{+, \times}^{ij} \left\{ a_i z_j + v_i v_j \right. \\ & + (\mathbf{n} \cdot \mathbf{x}) (z_i j_j + 3a_i v_j) + \frac{1}{c} \left[(\mathbf{n} \cdot \mathbf{v}) (a_i z_j + v_i v_j) \right. \\ & \left. \left. - (\mathbf{n} \cdot \mathbf{a}) v_i z_j - \frac{1}{2} (\mathbf{n} \cdot \mathbf{j}) z_i z_j \right] \right\}, \quad (7) \end{aligned}$$

where $n^i = x^i/r$ is a unit vector that points to the observer and vector product is the flat-space scalar product. In this case, we are neglecting terms of order $(v/c)^4$ and hence we are making a relative error of order $(v/c)^2$ with respects to the leading order quadrupole term.

The waveforms of equation (7) are a truncated multipole expansion, where we are neglecting the current-octopole, mass-hexadecapole, and higher multipole moments. This expansion is based on a slow-motion approximation which is valid for orbits whose pericenter velocity is small relative to the speed of light. For closed circular orbits, we can use the Virial theorem to argue

that this is equivalent to requiring $r_p > M_\bullet$. Since EMRBs are expected to have $r_p > 8M_\bullet$, this requirement is immediately satisfied. Moreover, since the octopolar contribution is of order v/c smaller than the quadrupolar contribution, for an EMRB event with $v_p/c = 0.4$, the maximum relative contribution of the octopole to the quadrupole is $\lesssim 40\%$.

4. NUMERICAL SIMULATIONS

In this section we describe the EMRB simulations that were carried out, including the choice of initial conditions. The simulations involve integrating the equations for geodesic motion around a Kerr black hole, equation (2), forward in time. (For a detailed exposition of Kerr geodesics see Chandrasekhar 1992). Since Cartesian Kerr-Schild coordinates are used, the initial conditions can be denoted by (z_0^i, v_0^i) . The numerical implementation does not use the Kerr geodesic constants of motion (energy, angular momentum, and Carter constant) in order to reduce the number of variables of the resulting system of ordinary differential equations. Instead, we have used the constants of motion to monitor the accuracy of the time integration. The integration accuracy is set so that we obtain fractional errors for the constants of motion smaller than one part in 10^{10} . The code uses a Bulirsch-Stoer extrapolation method as the evolution algorithm (see, e.g. Press et al. 1992; Stoer & Bulirsch 1993). We have also introduced in the code the possibility of switching between Kerr geodesics and Newtonian equations of motion. The gravitational waveforms are then obtained directly by applying expressions (6) and (7) to the numerically obtained trajectory $z^i(t)$.

Comparisons are carried out by choosing a representative relativistic orbit within the allowed phase space for EMRB's. We made the following choices for the test case:

- The central MBH mass is $M_\bullet = M_{\text{MW}}$ and the SCO mass is $m = 1 M_\odot$, such that the mass ratio is $\mu = m/M_\bullet = 2.5 \times 10^{-7} \ll 1$.
- The MBH spin parameter is either $a_\bullet = 0$ (Schwarzschild) or $a_\bullet = 0.998 M_\bullet$ (Kerr). The angular momentum is aligned along the z -axis and equal to either $S^z = 0$ or $S^z = 0.99GM_\bullet^2/c$.
- The observer is located at $r_{\text{obs}} = 8$ kpc along the z -axis, which corresponds to the approximate distance from Earth to the center of the Milky Way (Eisenhauer et al. 2005).

Furthermore, we make the following choices for the orbital initial conditions:

$$\begin{aligned} z_0^i &= (-1.59, 1.05, -0.185) \times 10^{-5} \text{ pc}, \\ v_0^i &= (1.70, -2.89, 0.510) \times 10^4 \text{ km s}^{-1}. \quad (8) \end{aligned}$$

The initial conditions are such that $r_0 = |z_0^i| = 50R_\bullet = 1.91 \times 10^{-5} \text{ pc}$, and $|v_0^i| = 0.11c = 3.39 \times 10^4 \text{ km s}^{-1}$. The orbital plane is inclined by 10° with respect to the $x - y$ plane to demonstrate the effects of orbital plane precession, which only take place for spinning MBHs.

The above orbit is representative of relativistic orbits within the EMRB phase space. For a Newtonian description of the central potential, the pericenter distance and

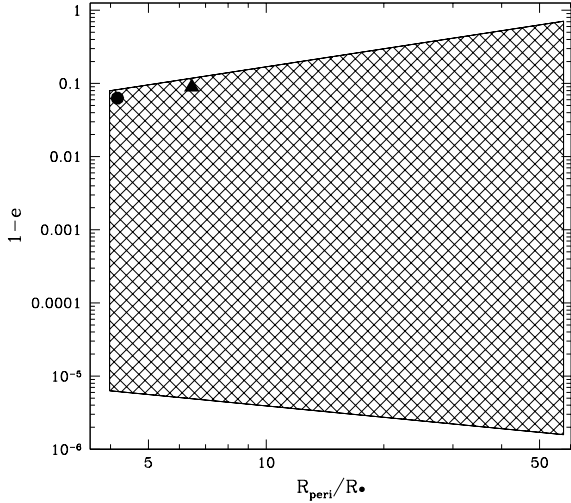


FIG. 1.— Plot of the pericenter distance in units of the gravitational radius R_* as a function of eccentricity for the initial data used in Rubbo et al. (2006, 2007). The initial conditions for the test and the extreme orbit correspond to the triangle and the circle respectively.

velocity would be

$$\begin{aligned} r_p &= 6.45 R_* = 2.48 \times 10^{-6} \text{ pc}, \\ |v_p| &= 0.384 c = 1.15 \times 10^5 \text{ km s}^{-1}. \end{aligned} \quad (9)$$

One might worry that with such high velocities, the SCO might be tidally disrupted. However, as shown by Hopman et al. (2006), most SCOs in EMRB scenarios consist of stellar-mass black holes, which cannot be tidally disrupted.

Relativistic orbits occur naturally in the phase space of possible EMRBs. The phase space probability contained within a small phase-space volume around the representative orbit is 6% using the same population models as in Rubbo et al. (2006, 2007). In Figure 1 we plot the pericenter separation in units of gravitational radii, R_* , as a function of the eccentricity, which was calculated assuming a Newtonian orbit. In this Figure, the orbit corresponding to equation (8) is given by a triangle. Although the orbit has a large eccentricity, the apocenter is small enough ($r_a \lesssim 150 R_* \approx 6 \times 10^{-5}$ pc) that the contribution from the surrounding stellar population to the potential can be neglected. In general, the left side of the figure corresponds to highly relativistic orbits with large pericenter velocities and small pericenter distances. Orbits with pericenter velocities $|v_p| > 0.25 c = 3 \times 10^4 \text{ km s}^{-1}$ account for approximately 50% of the possible orbits within the phase space.

Since the test orbit is a representative member of the relativistic region of the phase space, it will demonstrate the differences between the Newtonian and relativistic treatments. We could have chosen a more relativistic orbit that would still be classified as an EMRB event in a Newtonian treatment, but that would border with the definition of a continuous source. An example of such an extreme orbit is shown with a circle in Figure 1, to the left of the test orbit (triangle). This extreme orbit

possesses the following initial conditions:

$$\begin{aligned} x_0^i &= (-1.81, 0.6, -1.06) \times 10^{-6} \text{ pc}, \\ v_0^i &= (1.72, -1.78, 0.31) \times 10^5 \text{ km s}^{-1}, \end{aligned} \quad (10)$$

where $r_p = 4 R_* = 1.53 \times 10^{-6}$ pc and $|v_p| = 0.49c = 1.46 \times 10^5 \text{ km s}^{-1}$ for a Newtonian potential. We will study such an extreme orbit at the end of the next section as an example of a limiting relativistic case.

5. COMPARISON OF TRAJECTORIES AND WAVEFORMS

In this section we compare the results obtained for both the orbital motion and the gravitational radiation emitted by an EMRB event using both the Newtonian and relativistic description. Since the *plus* and *cross* polarization waveforms present similar features, we only plot the *plus* polarization waveforms. In the remainder of this section we use the following nomenclature: a quadrupolar (octopolar) Newtonian waveform is one that was calculated using the quadrupole (octopole) formula and Newtonian equations of motion; a quadrupole (octopole) Schwarzschild waveform is one that was calculated using the quadrupole (octopole) formula and the geodesic equations of motion with no spin ($a_* = 0$); a quadrupole (octopole) Kerr waveform is one that was calculated using the quadrupole (octopole) formula and the geodesic equations of motion with spin $a_* = 0.998 M_*$.

5.1. Orbital Trajectories

Let us begin by comparing the trajectories obtained in our simulations. In Figure 2, we plot the test orbit corresponding to a Newtonian treatment (solid line) and the one corresponding to a relativistic treatment without spin (dashed line) and with spin (dotted line). The dot and arrow indicate the initial location and velocity projected onto the x - y plane. The MBH is located at the origin of the coordinates, and the vectors denoted by L and S describe the direction of the initial orbital angular momentum and the MBH spin respectively. In the relativistic description there are precessional effects in the SCO orbit that can be clearly observed in Figure 2. These precessional effects are: pericenter precession about the orbital angular momentum axis, which acts in the initial orbital plane; and frame-dragging precession about the total angular momentum axis, which acts out of the initial orbital plane. While the former always occurs in a relativistic treatment, the latter is present only in the spinning case.

Different relativistic precessional effects are generally of different magnitude. In general, one finds that these effects are inversely proportional to the pericenter distance, or equivalently proportional to the pericenter velocity of the SCO. Precession out of the initial orbital plane, however, is smaller than precession in the orbital plane by a relative factor of order v_p/c and it is directly proportional to the spin of the MBH. In terms of post-Newtonian theory (see, e.g. Blanchet 2006), the pericenter advance is described by 1st-order post-Newtonian corrections to the equations of motion (order $(v/c)^2$ relative to the Newtonian acceleration), while precession off the orbital plane is due to spin-orbit and spin-spin couplings that correspond to 1.5 and 2-order corrections

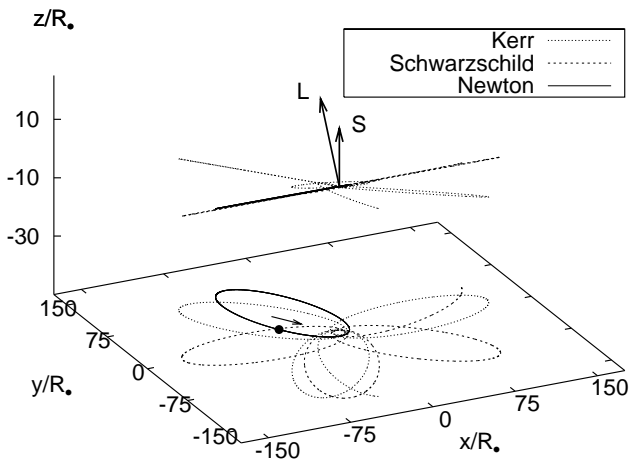


FIG. 2.— Trajectories for the SCO, with initial conditions given by (8), corresponding to a Newtonian description (solid line) and relativistic descriptions with no spin (dashed line) and with spin (dotted line). The MBH is located at the origin and the vectors L and S denote the initial orbital angular momentum and the MBH spin respectively.

(order $(v/c)^3$ and $(v/c)^4$ relative to the Newtonian acceleration.) Therefore, since EMRBs are characterized as events with small to moderate pericenter velocities, precession out of the initial orbital plane is small to moderate relative to pericenter advance, even for maximally spinning MBHs.

We can estimate the precession rate by comparing the Newtonian and relativistic trajectories. For the test orbit considered, we find that the rate in the orbital plane is roughly $\pi/3$ radians per orbit for the non-spinning case and $2\pi/3$ radians per orbit for the spinning one. These precessional effects have been studied extensively in the context of EMRIs (see, e.g. Schmidt 2002) and also specifically for S-stars in the central region of our Galaxy in Kraniotis (2007). Nonetheless, these effects have not been previously analyzed in the context of EMRBs which employed a quasi-Newtonian treatment. We shall discuss the consequences of such relativistic corrections as they are relevant to gravitational wave analysis below.

5.2. Waveforms

We now analyze how the differences in the SCO trajectories translate into different signatures in the waveforms. In Figure 3 we plot the quadrupole Newtonian and Schwarzschild waveforms (solid and dashed lines respectively), while in Figure 4 we plot the quadrupole Schwarzschild and Kerr waveforms (dashed and dot-dot-dashed lines respectively.) There are three main differences between the Newtonian and the relativistic waveforms: a phase change, an amplitude change, and a time of arrival change. The changes in amplitude and time of arrival are due to the test particle experiencing a larger “force” of attraction as it approaches the black hole. Quantitatively, this increase in force is due to the presence of (r_p^{-n}) -contributions to the relativistic corrections to the central potential (with n a real positive number.)

Gravitational wave interferometers are most sensitive to the phase, which is clearly different for Newtonian and

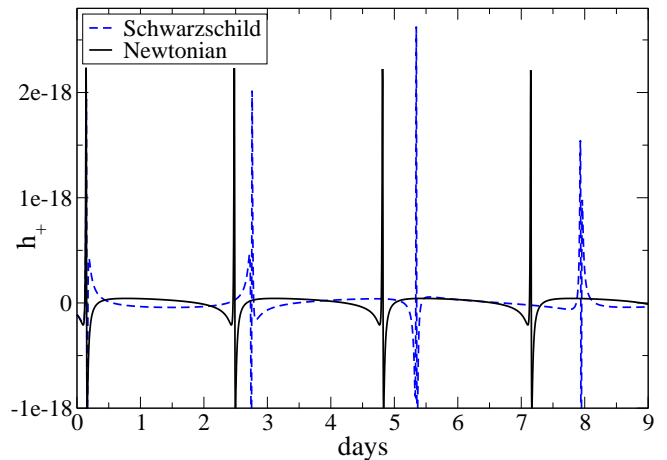


FIG. 3.— EMRB waveforms (*plus* polarization): The Newtonian waveform corresponds to the solid line and the Schwarzschild one to the dashed line.

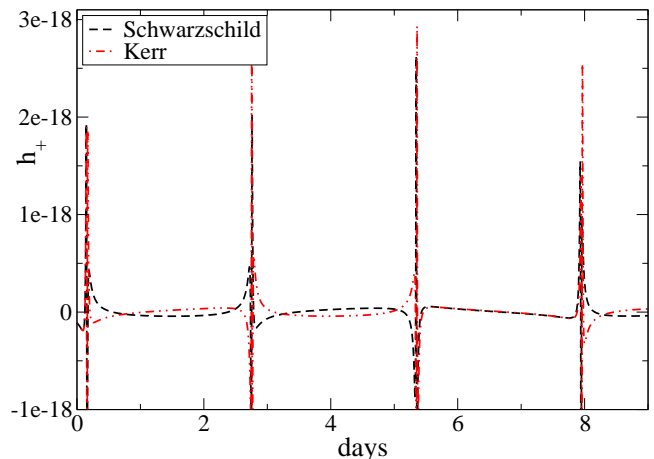


FIG. 4.— EMRB waveforms (*plus* polarization): The Schwarzschild waveform corresponds to the dashed line and the Kerr one to the dot-dot-dashed line. The dephasing of the waveforms can be best observed during the silent transitions between bursts. For example, in the first silent transition the waveforms are roughly π radians out of phase, while in the third one they are in phase.

relativistic waveforms. The dephasing present in Figures 3 and 4 parallels the orbital dephasing discussed earlier, since the gravitational wave frequencies are intimately related to the orbital frequency. In terms of the gravitational wave phase, both Figures 3 and 4 show a dephasing of $\pi/6$ radians per cycle. This can be seen after the third burst where the waveforms are back in phase. In fact, there is a significant dephasing even between the relativistic waveforms due to the effect of the MBH spin. If a cursory examination by eye can detect the difference in the waveforms due to differences in the nature of the central potential it is clear that strong EMRB waveforms can, in principle, be used as a probe of the spacetime near a MBH.

The difference in time of arrival and dephasing can be better studied by calculating the signal overlap,

$$(h_1|h_2) = \frac{\int_0^T h_1(t)h_2(t)dt}{\sqrt{\int_0^T h_1^2(t)dt} \sqrt{\int_0^T h_2^2(t)dt}}. \quad (11)$$

The overlap indicates how well a signal h_1 can be extracted via matched filtering with a template h_2 . In Fig-

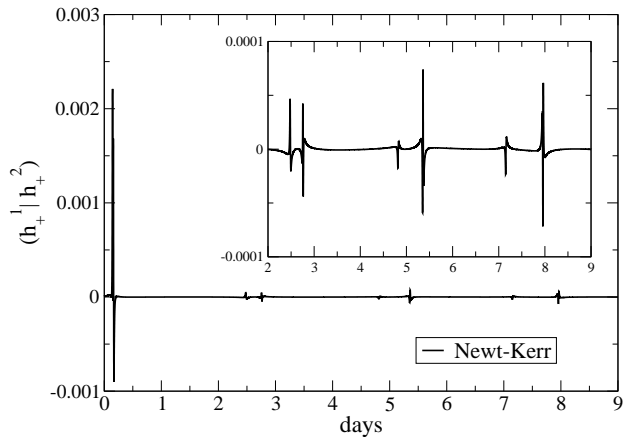


FIG. 5.— Plot of the overlap integrand of equation (11) with h_1 given by the quadrupole Kerr waveform and h_2 by the quadrupole Newtonian one. The inset zooms to a region near the small peaks.

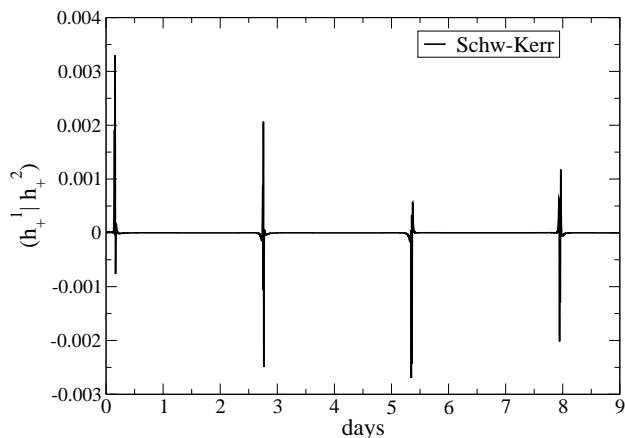


FIG. 6.— Plot of the overlap integrand of equation (11) with h_1 given by the quadrupole Kerr waveform and h_2 by the quadrupole Schwarzschild one.

ures 5 and 6 we plot the normalized integrand as a function of time, with h_1 given by the quadrupole Kerr waveform and h_2 given by either the quadrupole Newtonian or Schwarzschild waveforms. Observe that neither the Newtonian nor the Schwarzschild waveforms match well with the Kerr waveform. Moreover, note that the correlation with the Newtonian waveform deteriorates greatly after only the first cycle. These figures provide some evidence that for the data analysis problem of extracting EMRB signals, the use of a relativistic waveform might be required. We also calculated the integral of equation (11) and found that the correlation between the Newtonian and Kerr plus-polarized waveforms is 0.096, while the correlation between the Schwarzschild and Kerr plus-polarized waveforms is -0.063 . As a point of comparison, a substantial signal overlap should be $\gtrsim 80\%$.

Let us now study the differences in the waveforms when they are calculated with the quadrupolar approximation versus the quadrupolar-octopolar one. In Figure 7 we plot the absolute value of the difference between the octopole and quadrupole waveforms as a function of time and normalized to the maximum value of the Newtonian waveform ($h_N^{\max} \approx 2 \times 10^{-18}$.) The upper and lower panels present the results for the Schwarzschild and Kerr waveforms respectively. Observe that the inclusion of higher-order multipoles does not affect the phasing of

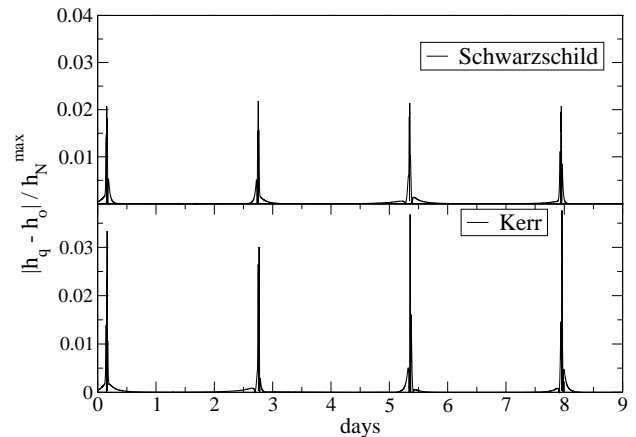


FIG. 7.— Plot of the absolute magnitude of the difference between the quadrupole and octopole Schwarzschild (upper panel) and Kerr (lower panel) waveforms. The difference is normalized to the rms value of the quadrupole waveform.

the waveforms, but only the amplitude, which is in general different by at most $\approx 4\%$ relative to the maximum of the Newtonian waveform. At first sight, this result is in disagreement with the expectation that the octopolar correction is $\lesssim 40\%$ of the quadrupolar one. Note, however, that the octopole correction is dependent on the location of the observer relative to the trajectory, velocity, acceleration and jerk vectors and, for an observer on the z -axis, it is actually reduced for the orbits studied by approximately an order of magnitude. Thus, the result is consistent with the expectation that the n -th multipolar contribution should be of order $(v/c)^n$ relative to the quadrupolar leading term.

5.3. Data Analysis

In order to quantify our statements about the change in phase and amplitude, we calculated the SNR for the relativistic waveforms via the standard formula

$$\rho^2 = 4 \int_0^\infty \frac{|\tilde{h}(f)|^2}{S_n(f)} df, \quad (12)$$

where the tilde denotes the Fourier transform and $S_n(f)$ is the one-sided power spectral noise density. Here we employ the Online Sensitivity Curve Generator (Larson et al. 2000) with the standard LISA settings and the inclusion of the white-dwarf background contribution. When calculating SNRs, we set the observation time to roughly nine days, so as to include multiple bursts in our single SNR value.

The inclusion of relativistic corrections in the trajectories has a dramatic impact in the SNR. We find that the Schwarzschild waveform increases the SNR by a factor of approximately 59%, while the Kerr waveform increases it by 162%, relative to the Newtonian SNR. The SNR increases because the relativistic orbits experience a deeper effective potential and, thus, the interaction timescale, $f_* = v_p/r_p$, is larger for the Schwarzschild and Kerr waveforms relative to the Newtonian one. As a result, the Fourier power shifted to higher frequencies, where LISA is more sensitive. Since the SNR is larger for relativistic waveforms, the event rate calculated in Rubbo et al. (2006, 2007) is clearly an underestimate for their galaxy model, because some of the systems with

a Newtonian SNR $\lesssim 5$ should have been added to the detectable event rate. However, the uncertainty in the event rate is probably dominated by astrophysical uncertainties and not by the dynamics modeling.

Conversely, the inclusion of higher multipole moments to the wave generation formalism had little to no effect in the SNR. In the previous section we showed that there was at most $\approx 4\%$ difference between the octopole and quadrupole waveforms relative to the maximum of the Newtonian one. Furthermore, we saw that this amplitude difference was confined to sharp peaks. Such a small and confined change in the waveform amplitude leads to a corresponding small change in the SNR: of the order of $\approx 1\%$ relative to the quadrupolar formalism. Therefore, we see that the increase in SNR is entirely dominated by the modifications introduced in the geodesic description of the equations of motion, and not in the octopolar correction to the waveform generation.

The analysis presented in this section, in particular Figure 5, makes it clear that relativistic corrections to the waveforms accumulate with multiple bursts. In other words, over a single burst (pericenter passage), a quadrupolar waveform calculation using Newtonian dynamics might be sufficient, even though one loses SNR. However, if one wants to estimate parameters associated with the central MBH, then multiple bursts must be associated to a single SCO trajectory. In terms of data analysis, for a detection search it is simpler to look for a single burst using techniques such as excess power and wavelet decompositions (e.g. see Anderson et al. 2001; Klimentenko et al. 2004; Stuver & Finn 2006; Camarda & Ortolan 2006). For estimating MBH parameters this paper suggests that multiple bursts must be connected. For this to occur, a single template may be used, but as our results indicate, the template will need to incorporate the effects of general relativity.

Let us conclude with some discussion of the parameters that might be extracted from these waveforms. Relativistic corrections can introduce strong modifications to EMRB waveforms. These corrections depend on how relativistic the EMRB event is and, in particular, on the pericenter velocity. The corrections are particularly strong for the class of EMRBs that inhabit the boundary between EMRBs and EMRIs, defined by the $T_{\text{cut}} = 3 \times 10^4$ s value, corresponding to the period between apocenter passages. An example of such an event is the extreme orbit discussed in Section 4, whose waveform is shown in Figure 8. Observe that a simplistic Newtonian description misses the rich structure, in which the SCO whirls twice about the black hole before zooming out to apocenter again. This behavior is missed entirely when we evolve the orbit with the Newtonian equations of motion, even though the same initial conditions were used.

Due to their whirling behavior, the extreme orbit waveform resembles the zoom-whirl events often mentioned in the EMRI literature (Hughes 2001a,b; Glampedakis & Kennefick 2002). However, the event is still an EMRB and not an EMRI because the period between apocenter passages is too long. For our galactic model, we find the probability of a small region of phase space around this orbit to be rather high, 10%. If this EMRB is detected with sufficiently high SNR it seems

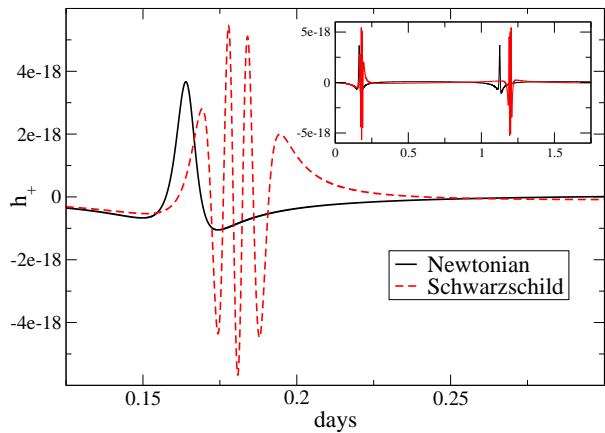


FIG. 8.— Plot of the quadrupole Newtonian (solid) and Schwarzschild (dashed) gravitational waveform as a function of time.

plausible that a parameter estimation analysis would allow for a determination of the background parameters, such as the black hole spin. Barack & Cutler (2004b) have already investigated LISA’s ability to measure MBH properties using approximate EMRI signals. They found that, depending on the actual orbital parameters, it will be possible to measure the MBH spin with fractional errors of 10^{-3} to 10^{-5} . This high precision measurement is the result of observing up to $\sim 10^6$ complete orbits. Conversely, it is very likely that EMRB measurements will not be able to match the measurement capabilities of EMRI signals, since only a few bursts will probably be available. Whether accurate parameter extraction is possible can only be determined with a more detailed data analysis investigation of EMRBs.

6. CONCLUSIONS

We have studied the effects of relativistic corrections on the gravitational waves produced by EMRBs. These events originate from long period orbits of a SCO around a MBH, leading to large-amplitude, quasi-periodic gravitational wave bursts. Using a more accurate relativistic treatment of the phenomenon, we have improved on the waveforms and trajectories relative to previous work. The orbital trajectories were corrected by accounting for the spacetime curvature of the system for Schwarzschild and Kerr MBHs. The waveform generation was corrected by accounting for the next order term in the multipolar expansion of gravitational radiation.

We found that relativistic corrections change the waveform shape relative to its Newtonian counterpart. One of the most significant changes was found to be a dephasing, produced by the relativistic corrections to the orbital trajectory and, in particular, by relativistic precessional effects. Other effects included a change in the amplitude of the waveform, partially produced by the inclusion of higher-order terms in the gravitational wave generation scheme.

The magnitude of the relativistic corrections was found to be directly proportional to the pericenter velocity of the orbit, as expected. Surprisingly, we estimated that at least 50% of the orbits analyzed in Rubbo et al. (2006, 2007) acquire relativistic velocities and, thus, non-negligible relativistic corrections. We investigated these corrections in detail by choosing a test orbit, which was found to be a representative member of the relativistic

sector of the EMRB phase space. We also studied a limiting case of a highly relativistic EMRB and found that it whirls more than once around the MBH before zooming back to apocenter and becoming silent again.

We have also discussed the possible consequences that relativistic effects might have on the detection and parameter estimation of gravitational waves from EMRBs by LISA. These effects have two main consequences on the data analysis pipelines: an increase in the SNR, and a dephasing due to relativistic precession. The SNR increase is mainly due to the relativistic treatment for the equations of motion, while a quadrupolar wave generation formalism seems to suffice. This finding is relevant particularly to match filtering searches, where a Newtonian treatment of the orbit would lead to a deterioration of the SNR and confidence limits. Furthermore, it seems possible that, given an EMRB gravitational wave detection, we might be able to extract or bound the spin of the central potential with a Kerr template. Other astrophysical consequences include an increase in the event rate, which implies that the rates of Rubbo et al. (2006, 2007) and Hopman et al. (2006) may be lower limits. However, the estimated event rates for EMRBs are still dominated by uncertainties in the astrophysical modeling for the host galaxy.

In addition to the astrophysical modeling, future research could be aimed in the data analysis and signal extraction direction for EMRB events. Based on the results of these studies, one may explore the possibil-

ity of testing alternative theories of gravity with EMRBs by performing matched filtering with templates from alternative theories (Will 1998; Scharre & Will 2002; Will & Yunes 2004; Berti et al. 2005b,a). Another possible avenue for future research is the study of confidence limits with which the spin of the central MBH can be measured. This research could then be used to examine whether EMRB events can distinguish (Collins & Hughes 2004; Glampedakis & Babak 2006; Barausse et al. 2007) between a pure Kerr MBH and a perturbed one (Yunes & Gonzalez 2006). Ultimately, these investigations will decide whether such events are worth studying in further detail by future gravitational wave observatories.

The authors would like to thank Ben Owen for reading the manuscript and providing useful comments. We would also like to acknowledge the support of the Center for Gravitational Wave Physics funded by the National Science Foundation under Cooperative Agreement PHY-01-14375, and support from NSF grants PHY 05-55628, PHY 05-55436, PHY 02-18750, PHY 02-44788, PHY 02-45649 and PHY 00-99559. K. H. B. and L. R. also acknowledge the support of NASA NNG04GU99G, NASA NN G05GF71G. C. F. S. acknowledges the support of the Natural Sciences and Engineering Research Council of Canada.

REFERENCES

- Amaro-Seoane, P., et al. 2007, ArXiv e-print astro-ph/0703495
 Anderson, W. G., Brady, P. R., Creighton, J. D. E., & Flanagan, E. E. 2001, *Phys. Rev.*, D63, 042003
 Babak, S., Fang, H., Gair, J. R., Glampedakis, K., & Hughes, S. A. 2007, *Phys. Rev.*, D75, 024005
 Barack, L., & Cutler, C. 2004a, *Phys. Rev. D*, 70, 122002
 —. 2004b, *Phys. Rev. D*, 69, 082005
 Barausse, E., Rezzolla, L., Petroff, D., & Ansorg, M. 2007, *Phys. Rev.*, D75, 064026
 Bender, P., et al. 1998, *Laser Interferometer Space Antenna for the Detection and Observation of Gravitational Waves: An International Project in the Field of Fundamental Physics in Space*, LISA Pre-Phase A Report, Max-Planck-Institut für Quantenoptik, Garching, mPQ 233
 Berti, E., Buonanno, A., & Will, C. M. 2005a, *Phys. Rev. D*, 71
 —. 2005b, *Class. Quant. Grav.*, 22, S943
 Blanchet, L. 2006, *Living Rev. Relativity*, 9, 4
 Camarda, M., & Ortolan, A. 2006, *Phys. Rev. D*, 74, 062001
 Chandrasekhar, S. 1992, *The mathematical theory of black holes* (New York: Oxford University Press)
 Collins, N. A., & Hughes, S. A. 2004, *Phys. Rev.*, D69, 124022
 Danzmann, K., & Rüdiger, A. 2003, *Class. Quant. Grav.*, 20, S1
 Eisenhauer, F., et al. 2005, *ApJ*, 628, 246
 Flanagan, E. E., & Hughes, S. A. 2005, *New J. Phys.*, 7, 204
 Gair, J. R., Kennefick, D. J., & Larson, S. L. 2005, *Phys. Rev. D*, 72, 084009
 —. 2006, *ApJ*, 639, 999
 Gair, J. R., et al. 2004, *Class. Quant. Grav.*, 21, S1595
 Ghez, A. M., et al. 2005, *ApJ*, 620, 744
 Glampedakis, K. 2005, *Class. Quant. Grav.*, 22, S605
 Glampedakis, K., & Babak, S. 2006, *Class. Quant. Grav.*, 23, 4167
 Glampedakis, K., & Kennefick, D. 2002, *Phys. Rev. D*, 66, 044002
 Holley-Bockelmann, K., & Sigurdsson, S. 2006, ArXiv e-print astro-ph/0601520
 Hopman, C., & Alexander, T. 2006, *ApJ*, 645, L133
 Hopman, C., Freitag, M., & Larson, S. L. 2006, ArXiv e-print astro-ph/0612337
 Hughes, S. A. 2001a, *Phys. Rev. D*, 64, 064004
 —. 2001b, *Class. Quant. Grav.*, 18, 4067
 Klimentenko, S., Yakushin, I., & Mitselmakher, G. 2004, *Class. Quant. Grav.*, 21, S1685
 Kraniotis, G. V. 2007, *Class. Quant. Grav.*, 24, 1775
 Larson, S. L., Hiscock, W. A., & Hellings, R. W. 2000, *Phys. Rev. D*, 62, 062001, <http://www.srl.caltech.edu/~shane/sensitivity/index.html>
 Marck, J.-A. 1996, *Class. Quant. Grav.*, 13, 393
 Misner, C. W., Thorne, K., & Wheeler, J. A. 1973, *Gravitation* (San Francisco: W. H. Freeman & Co.)
 Poisson, E. 2004, *Living Rev. Relativity*, 7, 6
 Press, W. H., Flannery, B. P., Teukolsky, S. A., & Vetterling, W. T. 1992, *Numerical Recipes: The Art of Scientific Computing* (Cambridge (UK) and New York: Cambridge University Press)
 Rubbo, L. J., Holley-Bockelmann, K., & Finn, L. S. 2006, *ApJ*, 649, L25
 Rubbo, L. J., Holley-Bockelmann, K., & Finn, L. S. 2007, in *Laser Interferometer Space Antenna: 6th International LISA Symposium*, ed. S. M. Merkowitz & J. C. Livas, Vol. 873 (AIP Conference Proceedings), 284–288
 Ruffini, R., & Sasaki, M. 1981, *Prog. Theor. Phys.*, 66, 1627
 Scharre, P. D., & Will, C. M. 2002, *Phys. Rev. D*, 65, 042002
 Schmidt, W. 2002, *Class. Quant. Grav.*, 19, 2743
 Stoer, J., & Bulirsch, R. 1993, *Introduction to Numerical Analysis* (New York: Springer-Verlag)
 Stuver, A. L., & Finn, L. S. 2006, *Class. Quant. Grav.*, 23, S733
 Sumner, T. J., & Shaul, D. N. A. 2004, *MPLA*, 19, 785
 Thorne, K. S. 1980, *Rev. Mod. Phys.*, 52, 299
 Tremaine, S., et al. 1994, *AJ*, 107, 634
 Will, C. M. 1998, *Phys. Rev. D*, 57, 2061
 Will, C. M., & Yunes, N. 2004, *Class. Quant. Grav.*, 21, 4367
 Yunes, N., & Gonzalez, J. A. 2006, *Phys. Rev.*, D73, 024010